

NUMERICAL SIMULATION ON EVOLUTION OF BOW WAVE OF KCS IN MOTION

ZHEN REN, DECHENG WAN

State Key Laboratory of Ocean Engineering, School of Naval Architecture, Ocean and Civil Engineering, Shanghai Jiao Tong University, Collaborative Innovation Centre for Advanced Ship and Deep-Sea Exploration, Shanghai, China

Keywords: Bow wave breaking, KCS, RANS, OpenFoam, surface tension

INTRODUCTION

The phenomena of wave breaking, known as white water, always occurs when ships advances in high speeds. The common issue has attracted many researchers since its complex mechanism and effects on the performance of ship. Since the shortages of towing experiments, such as expensive cost, insufficient information in flow field, et al. Computational fluid dynamics is becoming gradually a popular approach to study the overturning and breaking of ship bow wave. The advantage to provide detailed information in flow field is very helpful to understand better the mechanism of breaking wave.

The CFD solver naoe-FOAM-SJTU, which is developed on the open source software OpenFOAM, is used to investigate the wave breaking phenomena of the bow wave of KRISO Container Ship (KCS) model with sinkage and trim. URANS with high resolution VOF technique is adopted to simulate the bow wave breaking of KCS in different advance speeds, i.e. Fr=0.26, 0.35. The process of overturning and breaking of bow wave are captured clearly. The more detailed flow visualizations, such as wake profiles, vorticity and wave patterns, are presented to illustrate the hydrodynamic performance of high speed surface ship.

NUMERICAL METHOD

In the simulations, the governing equations mainly include the mass conservation equation Eqn (1) and the momentum equation Eqn (2), which can be written as:

The mass conservation equation:

$$\nabla \cdot \mathbf{U} = 0 \quad (1)$$

The moment conservation equation:

$$\frac{\partial \rho \mathbf{U}}{\partial t} + \nabla \cdot [(\rho \mathbf{U} - \mathbf{U}_g) \mathbf{U}] = -\nabla p_d - \mathbf{g} \cdot \mathbf{x} \nabla \rho + \nabla \cdot (\mu_{\text{eff}} \nabla \mathbf{U}) + (\nabla \mathbf{U}) \cdot \nabla \mu_{\text{eff}} + f_{\sigma} \quad (2)$$

Where \mathbf{U} is fluid velocity field and \mathbf{U}_g is the grid velocity; p_d represents the dynamic pressure; ρ is the mixture density; g is the gravity acceleration; μ_{eff} is effective dynamic viscosity, in which ν and ν_t are kinetic and eddy viscosity, respectively, and ν_t is obtained from turbulence model. f_{σ} is surface tension term that plays an important role in wave breaking simulation. SST $k-\omega$ model[1], is selected to solve the Reynolds stress. k denotes turbulence kinetic energy and ω denotes dissipation rate. The turbulence model combines the advantages of the standard $k-\epsilon$ model and $k-\omega$ model to make sure that the free surface is not influenced and ensure the accuracy and reliability of the solution at the wall.

Here the Volume of Fluid (VOF) method with artificial compression [2] is used to capture the free surface. According to the literature concerning wave breaking, small scale wave breaking is strongly influenced by surface tension. The role played by the surface tension is quite different for breaking and non-breaking waves since the surface tension pressure jump depends on the magnitude of the radius of curvature of the free surface. In order to reappear the wave patterns of the experiment, the surface tension is taken account in the present simulation and the surface tension term mentioned in Eqn(3). is expressed as:

$$f_\sigma = \sigma \kappa \nabla \alpha \tag{3}$$

Where σ stands for the surface tension, κ is the curvature of free surface and it is defined as:

$$\kappa = -\nabla \cdot \mathbf{n} = -\frac{\sum_f \mathbf{S}_f \cdot \mathbf{n}_f}{V_i} \tag{4}$$

V_i represents the volume of cell i , $\sum_f \mathbf{S}_f$ stands for the sum of value on each face of cell.

The geometry of KCS model ($L_{pp}=6.0702\text{m}$, with rudder) can be obtained in the workshop on CFD in ship hydrodynamics, Tokyo 2015. In the experiments, the model has two degrees of freedoms, sinkage and pitch (positive, trim by stern). In the simulation, both degrees of freedoms are considered.

VALIDATION OF NUMERICAL SCHEME

The focus of the present study is on the resolution of bow wave breaking of KCS at different speeds, i.e. $Fr = 0.26, 0.35$. The condition at $Fr = 0.26$ is selected to validate the prediction accuracy of the current numerical scheme. Table 1 shows the comparison of the predicted resistance, sinkage and pitch with the experiment data. The error of resistance, sinkage and pitch are less than 0.6%, 6%, 3%, respectively. Figure 1 shows the wave height of the three profiles ($y/L = 0.0741, 0.1509, 0.4224$), obtained by experiment and numerical simulations. From the near field to the far field, the calculated free surface is consistent with the experimental measurements. The wave profiles on hull surface achieved by numerical method and experiment data are shown in Figure 2. Except for the deviation of the bow and stern wave, the other results are in good agreement with the experimental measurements. The above results prove that the numerical scheme in the present work is reliable.

Table 1. Comparison of prediction and experimental data

Parameter	EFD	CFD	Error
Resistance(N)	52.18	51.88	-0.57%
Sinkage(/m)	-0.01259	-0.01191	-5.36%
Pitch(°)	-0.1646	-0.16925	2.82%

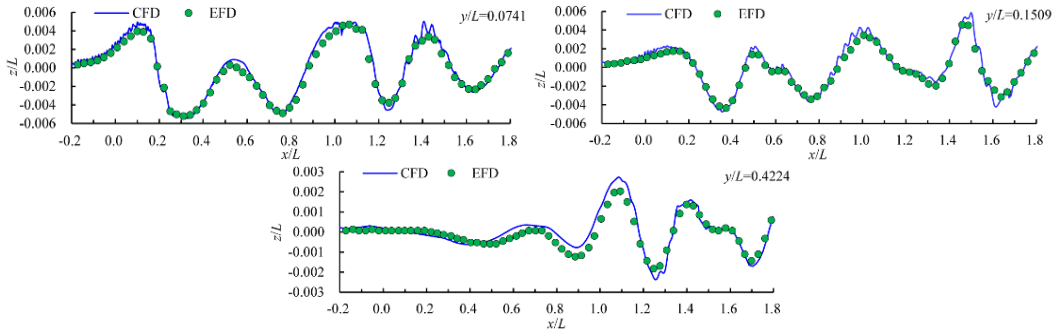


Fig 1. Comparison of Free-surface cuts between experiments (circles) and computational results(line) at different positions.

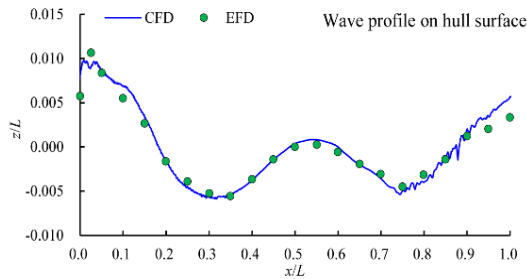


Fig 2. Wave profile on hull surface

RESULTS & ANALYSIS

Although the advance speed of KCS will not reach $Fr=0.35$ in the actual voyages, the phenomenon of bow wave breaking is only observed at high speeds.

Table 2 presents the prediction of resistance and motion of KCS at $Fr=0.35$. Compared with the values of KCS at $Fr=0.26$, the resistance increases rapidly and the sinkage shows the same trend. The pitch at $Fr=0.35$ is less than that at $Fr=0.26$, as presents that the trim by bow of KCS is reduced. The velocity vector at different cutting planes in the evolution of bow wave breaking are presented in Fig.3. At $x/L=0.06$, the initial plunger is generated since the interaction between gravity and inertial forces. The higher velocity is concentrated at the tip of initial plunger which move downward. The initial plunger has reconnected with the below surface at $x/L=0.07$. At $x/L=0.095$, the second plunger is going to be formed. The higher velocity is concentrated near upper edges of the reconnection region.

Table 2. Prediction at $Fr=0.35$

Parameter	Resistance(/N)	Sinkage(/m)	Pitch(°)
Value	70.20	-0.01894	-0.07704

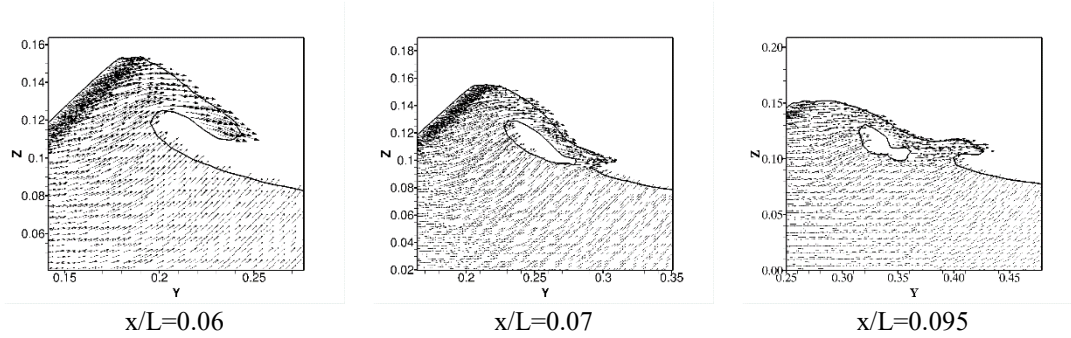


Fig.3 Velocity vector at different cutting plane

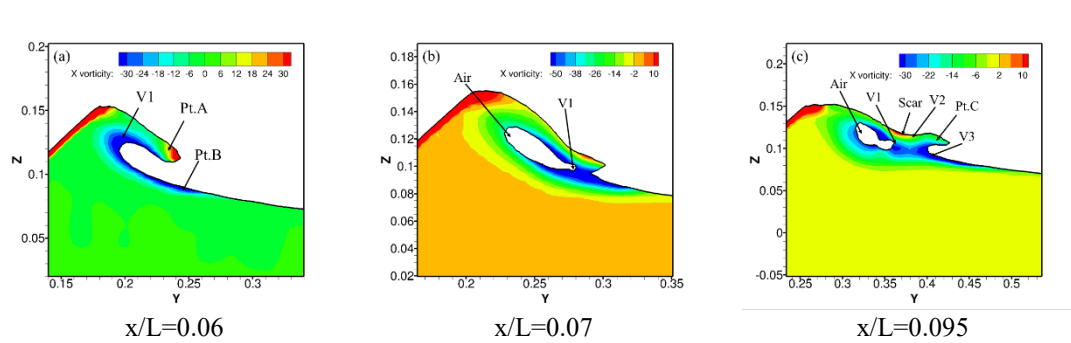


Fig.4 Axial vorticity distribution

Fig.4 presents the axial vorticity at $x/L=0.06$, 0.07 and 0.095 , respectively. As shown in Fig.4 (a), the Pt.A represents the initial plunger that is generated due to the interaction between gravity and inertial forces. The reconnection between the initial plunger and the free surface below (represented by Pt.B) will happen along with the development of initial plunger outboard. In the high curvature region of the overturning wave, the negative axial vorticity (labeled as vortex V1) is generated in the process that the initial plunger is falling. When the tip of initial plunger reconnects with the free surface below, air will be entrained, as shown in Fig.4 (b), resulting in more complex phenomena.

The generation of the counter-rotating vortex pair (V2 and V3) at $x/L=0.095$ is responsible for the scar where the positive vorticity (V2) is generated and the second plunger visible at $x/L=0.095$. When the tip of the initial plunger reconnects with the free surface below, the interaction between the two parts causes the upward motion of fluid resulting in the positive vorticity and scar (V2, Scar in Fig4(c)) and the negative vorticity (V3) is generated at the toe. The vortex pair that has a rotating orientation pumps fluid outboard resulting in the second plunger. The air entrainment is observed at $x/L=0.07$, 0.095 in the process of the overturning of the initial plunger.

CONCLUSION

In the present work, an exploratory study on the wave breaking of KCS under high speed is performed. The overturning and breaking of bow wave is observed clearly and also the air entrainment and scar are noticeable. In the process of the overturning of bow wave, the variation of vorticity is concentrated near the free surface. The counter-rotating vortex generated by the reconnection of the initial plunger with the

free surface below is responsible for the second plunger and scar. In the present study, the reference of grid scale to simulate the wave breaking is provided. But the use of the present scheme does not allow for a very elaborate simulation of bow wave breaking. So, in the future work, smaller grid size may be adopted. In addition, the phenomenon of air entrainment that is captured roughly in the present study should be paid more attention, such as, the evolution downstream and outboard.

ACKNOWLEDGMENTS

This work is supported by the National Natural Science Foundation of China (51379125, 51490675, 11432009, 51579145), Chang Jiang Scholars Program (T2014099), Shanghai Excellent Academic Leaders Program (17XD1402300), Program for Professor of Special Appointment (Eastern Scholar) at Shanghai Institutions of Higher Learning (2013022), Innovative Special Project of Numerical Tank of Ministry of Industry and Information Technology of China (2016-23/09) and Lloyd's Register Foundation for doctoral student, to which the authors are most grateful.

REFERENCES

- [1] Menter, FR, Kuntz, M, Langtry, R (2003). "Ten years of industrial experience with the SST turbulence model, Turbulence," *Turbul Heat Mass Transf*, 4(1), 625-632.
- [2] Weller, H and Weller, H (2008). "A high-order arbitrarily unstructured finite-volume model of the global atmosphere: Tests solving the shallow-water equations," *Int J Numer Methods Fluids*, 56(8), 1589-1596.